Trans. Nonferrous Met. Soc. China 25(2015) 1704−1714

Formation and sedimentation of Fe-rich intermetallics in Al−Si−Cu−Fe alloy

Wen-chao YANG[1,2], Feng GAO[2], Shou-xun JI[2]

1. State Key Laboratory of Solidification processing, Northwestern Polytechnical University, Xi'an 710072, China
2. Brunel Centre for Advanced Solidification Technology, Brunel University London, Uxbridge, Middlesex UB8 3PH, United Kingdom

Received 20 June 2014; accepted 7 November 2014

Abstract: Formation and sedimentation of Fe-rich intermetallics were studied in a commercial Al−Si−Cu−Fe alloy with extra additions of Mn. It is found that the introduction of extra Mn is an effective approach to lower the Fe level in the equilibrium liquid phase after sedimentation of solid Fe-rich phase at a temperature between its liquidus and solidus. The higher Mn/Fe mass ratio results in the lower Fe content in the retained alloy, during which Mn is also consumed and settled at the bottom of the melt as solid Fe-rich intermetallics. Therefore, the final Fe content in the alloy can be controlled by the Mn content and the holding temperature of the melt. The results confirmed a good agreement of the theoretical calculation and the experimental test with a specially designed 50 mm cylindrical casting. The sedimentation of Fe-rich intermetallics in the Al−Si−Cu−Fe alloy is completed at 600 °C after 10 min. The reduction of Fe content in the retained alloy is 31.4% when m(Mn)/m(Fe)=0.5 and 53.3% when m(Mn)/m(Fe)=1.0 in comparison with that in the original alloy. The settled Fe-rich intermetallics were identified as α-$Al_{15}(Fe,Mn)_3Si_2$, which provided the lower balanced Fe concentration in the melt in comparison with other Fe-rich intermetallics.
Key words: aluminium alloy; solidification; intermetallics; iron removal

1 Introduction

Aluminium alloys have been extensively used in foundry practice for manufacturing structural components. They are always regarded as being completely recyclable, which represents one of the key attributes of this ubiquitous metal with far-reaching economic, ecological and social implications [1,2]. However, a major concern in recycled aluminium alloys is the concentration increase of some elements that have been identified to be detrimental on the mechanical properties. One of the most significant elements is iron, which is easily picked up during casting operation either from the high iron-containing scraps/contamination or from the steel tools used in production. Because Fe has a low solubility in aluminium, it reacts with Al and Si to form a variety of intermetallic compounds during solidification [3,4]. These brittle Fe-rich intermetallics in aluminium alloys can act as the resource of cracks under loading and therefore decrease the strength and ductility of the final products [5,6]. Therefore, the minimization of detrimental effect of Fe-rich intermetallics has been one of the active research areas in past several decades, in which removal of iron from aluminium melt, dilution of the secondary aluminium melt with primary aluminium, and applying a classification to scraps prior to melting are commonly used as industrial solutions.

Several techniques of iron removal from aluminium melt have been developed in past several decades in order to reduce the iron levels in the recycled aluminium alloys [7]. However, most of these methods are still in laboratory research for fundamental understanding. The formation of iron-rich intermetallic phases in aluminium melt is a fundamental for iron removal during recycling. In the conventional and popular practice, aluminium alloys are maintained at a temperature below its liquidus, which allows the sedimentation of Fe-rich intermetallics, followed by a physical separation of liquid and solid phase. Obviously, the sedimentation is controlled by the amount of Fe-rich intermetallics formed at the holding temperature. It has been confirmed that a variety of Fe-rich intermetallic phases can be observed in aluminium alloys. In Al−Si−Fe system there are five main Fe-rich phases: Al_3Fe (or $Al_{13}Fe_4$), α-Al_8Fe_2Si (possibly α-$Al_{12}Fe_3Si_2$), β-Al_5FeSi, δ-Al_4FeSi_2 and γ-Al_3FeSi [8,9]. In hypoeutectic Al−Si alloys containing Fe, Mn and Mg, three Fe-rich phases named as

Corresponding author: Shou-xun JI; Tel: +44-1895-266663; Fax: +44-1895-269758; E-mail: shouxun.ji@brunel.ac.uk

α-$Al_{15}(Fe,Mn)_3Si_2$, β-Al_5FeSi and π-$Al_9FeMg_3Si_5$ compounds have been identified [10,11]. In the commonly used Al−Si−Mg cast alloys, the Fe-rich intermetallic is believed as the body centred cubic α-$Al_{15}(Fe,Mn)_3Si_2$ when Mn/Fe mass ratio is over 0.5 and β-Al_5FeSi phase when Mn/Fe mass ratio is below 0.5 [12]. The Mn/Fe mass ratio has been identified as sludge factor in aluminium alloys [13,14]. The recent study has shown that the Fe-rich intermetallics are α-AlFeSi and β-AlFe in Al−Mg−Si cast alloy [6]. According to the principle of thermodynamics, because of the difference between structure and formation temperatures for various types of Fe-rich intermetallic phases, the balanced Fe concentration in the liquid phase should be different. However, it is still not very clear how Fe is balanced between the solid intermetallics and the liquid phase, although Fe has been commonly believed to be precipitated in the sedimentation sludge.

On the other hand, manganese has been known to suppress the formation of long needle-shaped Fe-rich phases and to promote the formation of compact Fe-rich phases in aluminium alloys [6]. It had been found that Mn could enlarge the area of forming α-AlFeMnSi phase in the equilibrium phase diagram of an Al−Mg−Si−Mn alloy and thus the α-$Al_{12}(Fe,Mn)_3Si$ phase could be obtained at a higher Fe level by controlling the Mn content in the melt. In the meantime, the composition of β-AlFe phase was identified as $Al_{13}(Fe,Mn)_4Si_{0.25}$ in the same alloy, which was formed at even higher Fe content. These results indicated that the addition of Mn could alter the solidification path and promote the formation of intermediate Fe-rich phase in the melt, which was able to reduce the balanced content of iron in the liquid phase. This is particularly important if the remained Mn is still within the specification requirement after adding extra Mn for Fe removal. More importantly, during recycling of Al alloys, the Fe level in the retained alloys should be controlled at an acceptable level, rather than the lowest level because of the economical limitation and the requirement for different applications. Therefore, more works are necessary to consolidate the fundamental understanding of the formation of Fe-rich intermetallics in aluminium melt with Mn addition and the microstructural characterization of different phases in the retained Al alloys and in the sedimentation materials. The combination of thermodynamics calculation and CALPHAD modelling with the experimental evidence for the formation of intermediate phases in aluminium alloys will provide fundamental understandings for Fe-rich intermetallics in the liquid phase and in the solid phase, which is a useful guidance for technological development of iron removal.

The present study aims to investigate the formation and sedimentation of Fe-rich intermetallic phases in Al−Si−Cu−Fe alloy with increasing Fe content and different levels of Mn addition using thermodynamics calculation and CALPHAD modelling. The relationship between the added Mn and the remained Mn content in the alloy after sedimentation of Fe-rich intermetallics will be set up for industrial application. The experimental determination of Fe content in the retained alloy is achieved by analyzing the alloy composition at different positions of cylindrical castings under different solidified conditions. The discussion is focused on the solidification, microstructural evolution and the sedimentation process during holding the melt in the solid−liquid co-existing state.

2 Experimental

Commercial A380 alloys with the composition of Al−8.3%Si−3.46%Cu−1.90%Zn, Al−20%Mn and Al−80%Fe master alloys were used to make experimental Al−Si−Cu−Fe alloys to simulate the recycled materials by adding Fe element and to examine the formation of α-AlFeMnSi intermetallics by adding different levels of Mn in the melt. 8−10 kg melt was prepared in a SiC crucible located in an induction furnace. The alloy was melted at 750 °C for 30 min before taking sample for composition analysis. A d50 mm×60 mm cylindrical sample was made by casting the melt directly into a steel mould for the composition analysis. The casting was cut across the diameter at 15 mm from the bottom and ground down to 800 grid abrasive grinding paper. The alloy composition was obtained by an optical mass spectroscope, in which at least four spark analyses were performed and the average value was taken as the chemical composition of the alloy. Some elements were further confirmed by area energy dispersive X-ray (EDX) quantification with scanning electron microscope (SEM). The alloy compositions used in current research were analyzed as shown in Table 1, in which the major difference was the Mn content and the other elements were essentially at the same level.

After composition analysis, the melt was manually filled into a d50 mm×2500 mm cylindrical metal mould

Table 1 Alloy compositions with different Mn additions used in experiment (mass fraction, %)

Alloy	Si	Fe	Mn	Cu	Zn	Others	Al
A	8.3±0.08	1.0±0.05	1.0±0.04	3.5±0.06	1.9±0.1	0.3±0.06	Bal.
B	8.3±0.08	1.0±0.05	0.5±0.05	3.5±0.06	1.9±0.1	0.5±0.05	Bal.

with a wall thickness of 2 mm. The internal surface of the mould was coated by BN coating and dried at 200 °C. The pouring temperature was 650 °C measured by a K-type thermocouple. The castings were made by two different methods. In the first method, the melt was cooled directly and continuously cooled from 650 °C to ambient temperature to form castings without interruption and extra processing, which was referred as conventional castings. By the second method, the melt was cooled from 650 to 600 °C and then controlled isothermally at 600 °C for different time, followed by quenching the alloy with mould into a water tank with constant water flowing. This was referred as sedimentation castings.

To test the chemical composition at different locations in the castings, each cylindrical casting was cut radically into two halves. Then one half was used for composition analysis. The longitudinal section was ground down to 800 grid abrasive grinding paper before analyzing the composition with the same optical mass spectroscope as described above. The centre of each spark burning mark was taken as the location of analysis and the average value of three castings was taken as the final composition of each location.

The specimens for microstructure characterization were taken from the same location as for the composition analysis. Following a standard procedure of grinding and polishing, the specimens were examined by a Zeiss optical microscopy with an AxioVision 4.3 Quantimet digital image analysis system and a Zeiss SUPRA 35VP SEM, equipped with EDX. The quantitative EDX analysis in SEM was performed at an accelerating voltage of 20 kV on a polished sample, and the libraries of standard X-ray profiles for EDX were generated using pure elements. In situ spectroscopy calibration was performed in each session of the EDX quantification using pure copper. To minimize the influence from the interaction volume during the EDX quantification, five point analyses on selected particles were conducted for each phase and the average was taken as the measurement.

3 Results

3.1 Thermodynamics calculation of multi-component Al−Si−Cu−Fe−Mn system

In order to understand the effect of alloying elements on the solidification and microstructural evolution, the multi-component Al−Si−Cu system with varied Mn and Fe was thermodynamically calculated using Pandat software [15], where the α-AlFeMnSi was treated as a stoichiometric phase during the modelling. The calculated equilibrium phase diagram on the cross sections of Al−8.3Si−3.5Cu−1.9Zn−xMn−yFe is shown in Fig. 1. It was seen that the calculated equilibrium phase diagram could be divided into several regions with different levels of Fe contents. When the Mn addition was at 0.5%, the phase formation could be described as

$L\rightarrow\alpha$-AlFeMnSi+α-Al+Si+θ-Al_2Cu, w(Fe)<1.35%

$L\rightarrow\alpha$-AlFeMnSi+β-AlFeSi+ α-Al+Si+θ-Al_2Cu, w(Fe)>1.35%

In both situations, α-AlFeMnSi phase was the prior phase, although the subsequent solidification would form different types of phases. When the Mn content was increased to a higher level of 1.0%, the solidification process could be described as

$L\rightarrow\alpha$-AlFeMnSi+α-Al+Si+θ-Al_2Cu, w(Fe)<2.0%

$L\rightarrow\alpha$-AlFeMnSi+β-AlFeSi+α-Al+Si+θ-Al_2Cu, w(Fe)>2.0%

It was seen that the prior α-AlFeMnSi phase showed no change, but the formation range was enlarged to 2.0% Fe, representing an increase of 65%. This was further confirmed by the increase of Mn content to 2.0% Mn, the solidification could be also divided into two areas and could be described as

$L\rightarrow\alpha$-AlFeMnSi+α-Al+Si+θ-AlCu, w(Fe)<3.2%

$L\rightarrow\alpha$-AlFeMnSi+β-AlFeSi+α-Al+Si+θ-AlCu, w(Fe)>3.2%

It should be noted that the formation of β-AlFeSi phase in the as-cast microstructure was also significantly affected by the Mn content in the alloy, which started from 1.35% Fe when Mn content was 0.5%, and from 2.0% Fe when Mn content was 1.0% in the experimental alloys.

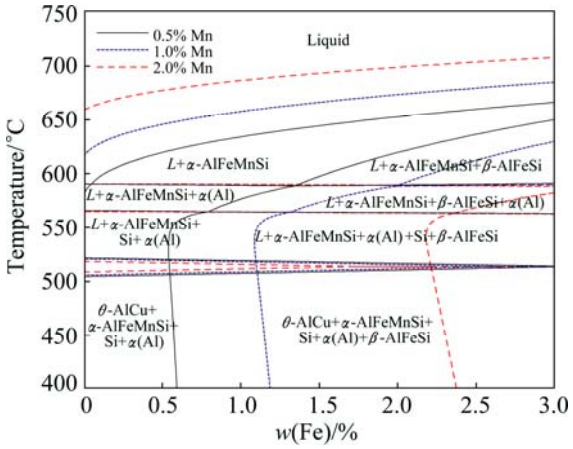

Fig. 1 Equilibrium phase diagram of Al−8.3%Si−3.5%Cu−1.9%Zn alloy with different Fe and Mn contents

According to the equilibrium phase diagram as shown in Fig. 1, Mn increased the area of forming α-AlFeMnSi intermetallic compound in the alloy. With three levels of Mn contents of 0.5%, 1.0% and 2.0%, it

was seen that the liquidus line of α-AlFeMnSi formation was moved to higher temperatures for the increased Mn content in the alloy. This confirmed that the addition of Mn increased the liquidus temperature of alloys. It was also seen that the Fe content to form β-AlFeSi phase was also raised to higher values with the increase of Mn content in the alloy. In other words, with the increase of Mn content in the alloy, the α-AlFeMnSi phase was formed as prior phase at a lower level of Fe content in the alloy. Therefore, the processing window to form the α-AlFeMnSi phase was significantly enlarged with the increase of Mn content in the alloy. In the meantime, it was seen that the addition of Mn reduced the equilibrium concentration of Fe in the liquid aluminium melt. This was important as it indicated that Fe content in the melt could be controlled through the addition of Mn into the alloy, which provided the fundamentals for the iron removal in aluminium alloys.

The variation of Fe, Mn and Si contents during solidification could be understood more clearly by calculating the equilibrium concentration in the liquid with different Mn/Fe mass ratios. The results are shown in Fig. 2, where the calculated equilibrium concentrations of Si were located at the upper left corner as inserts. It was seen that the balanced concentrations of Fe and Mn in the liquid phase were significantly reduced with the decrease of the temperature in the interval of liquidus and solidus. When m(Mn)/m(Fe)=0.5 in Fig. 2(a), the equilibrium concentration of Fe was decreased from 1.05% to 0.72% at 600 °C in the liquid phase. In the same time, the initial content of 0.5% Mn at 650 °C was decreased to 0.2% Mn at 600 °C in the liquid phase, showing a significant reduction. However, the content of Si only showed a slight reduction from 8.34% to 8.26% at 600 °C in the liquid phase. The results confirmed that Mn and Fe contents could be significant altered while the Si content kept constant in the alloy. The similar situation could also be observed when m(Mn)/m(Fe) was set at 1.0. The equilibrium Fe content was decreased from initial 1.05% at 650 °C to 0.49% at 600 °C. The equilibrium Mn content was decreased from 1.02% at liquidus temperature to 0.27% at 600 °C. Similarly, the Si content did not show significant change in the same temperature variation. It was 8.34% at liquidus temperature and 8.22% at 600 °C. From these calculations, it was confirmed that Si content had no obvious variation with different levels of Mn in the alloy. However, the increase of m(Mn)/m(Fe) ratio resulted in a significant decrease of Fe content in the liquid phase of alloy when it was maintained at a temperature between the liquidus and the solidus. Therefore, Fe content in the liquid could be controlled by adjusting the m(Mn)/m(Fe) ratio and temperature in practical operation.

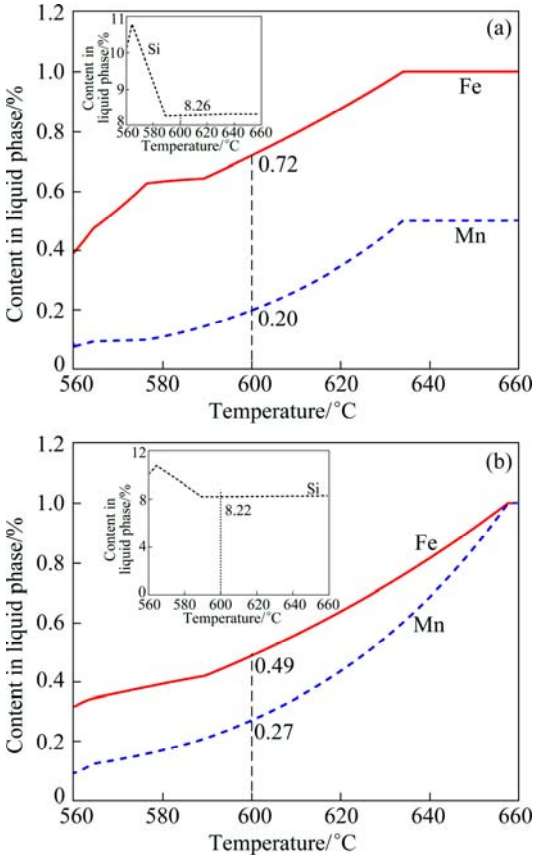

Fig. 2 Equilibrium concentration of Fe, Mn and Si in liquid phase of alloy A during solidification, calculated from equilibrium phase diagram: (a) m(Mn)/m(Fe)=0.5; (b) m(Mn)/m(Fe)=1.0

3.2 Composition variation in Al−Si−Cu−Fe alloy during processing

Figures 3(a)−(c) respectively showed the content changes of Fe, Mn and Si on a longitudinal section of continuously cooling from 650 °C to room temperature in alloy A with m(Mn)/m(Fe)=1.0. It was seen that although the contents of these elements presented a very slight increase from the top to the bottom of the casting, their content is close basically to the original content, indicating a basic uniform distribution of solute elements across the longitudinal section on the cylindrical casting when alloy A was directly cooled from a temperature above the liquidus to the ambient temperature. It was also confirmed that there was no obvious sedimentation for the Fe-rich intermetallics in the conventional casting under normally solidified condition. However, if the alloy was maintained at a temperature between the liquidus and the solidus, the prior phase α-AlFeMnSi was formed and then settled at the bottom of the liquid because of the density difference between the solid α-AlFeMnSi phase and the liquid aluminium phase. Figure 4 showed the contents of Fe, Mn and Si along a longitudinal section of the sedimentation casting for alloy A, which was maintained at 600 °C for different

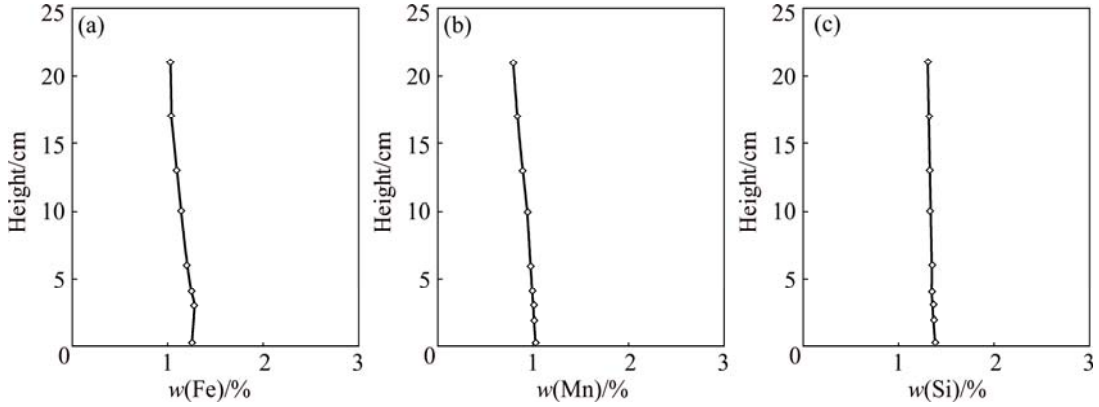

Fig. 3 Contents of Fe (a), Mn (b) and Si (c) along radial cross section of *d*50 mm × 250 mm casting made by continuously cooling of alloy A from 650 °C to room temperature (conventional solidification)

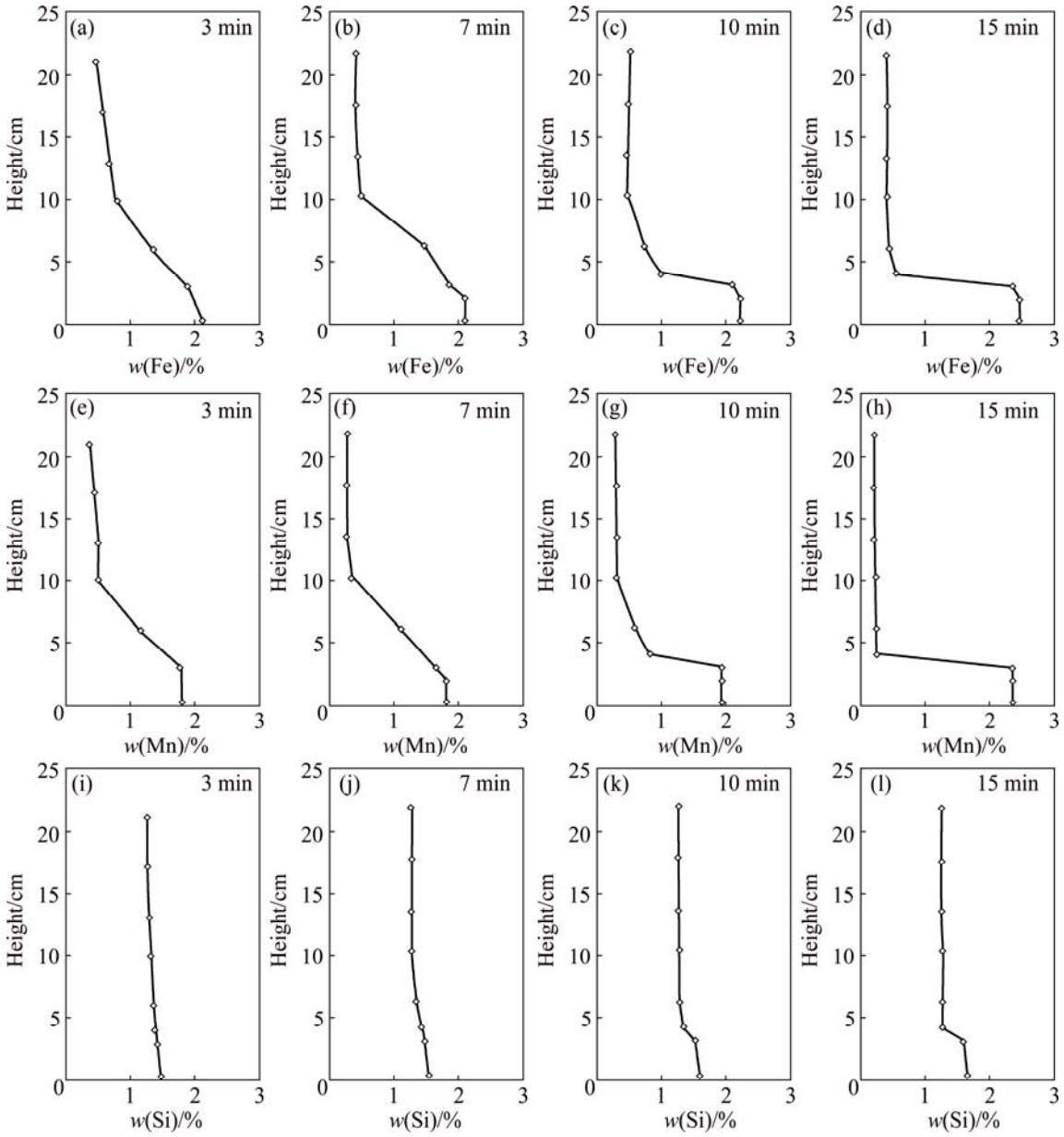

Fig. 4 Contents of Fe, Mn and Si along radial cross section of *d*50 mm × 250 mm casting made by alloy A continuously cooled from 650 °C to 600 °C and isothermally maintained at 600 °C for different time, followed by water quenching of alloy with mould at 3, 7, 10 and 15 min

time. With the prolonged holding at 600 °C, the Fe-rich intermetallics were gradually settled at the bottom of the cylindrical casting. After 10 min, solid Fe-rich intermetallics were almost settled at the bottom of the casting. The iron content in the liquid at the top of the cylinder casting was obviously much lower than the initial content. With the further increase of holding time, the depth of the low Fe and Mn layer was increased. It was seen that a clear and steep line exists near the bottom of the casting to show the difference of the contents of Fe and Mn. In comparison with the results shown in Fig. 3, it was clear that the contents of Fe and Mn in the liquid phase were consistently close to the equilibrium values shown in the phase diagram. The detail variations between the experimental results and the calculated equilibrium values were summarized in Table 2. In addition, the similar experiments were also performed for alloy B with m(Mn)/m(Fe)=0.5. As seen from Table 2, it presented a clear consistency between experimental and calculated values no matter which one alloy was analyzed. On the other hand, the Si content showed no obvious difference with prolonged holding at 600 °C, although it was measured the clear difference of the Si content in the solid α-AlFeMnSi phase and in the balanced aluminium liquid phase. For m(Mn)/m(Fe)=1.0 alloy, after 10 min sedimentation, the Si content was 8.27% at the top of the cylindrical casting, which was recognized as retained alloy, and 8.58% at the bottom of the cylindrical casting, which is recognized as sedimentation alloy. It was seen that the difference for Si content was not significant, only reduced from 8.34% to 8.27%. This was actually within the error tolerance of measuring equipment.

Table 2 Contents of Fe, Mn and Si in melt obtained by CALPHAD calculation and experiment

m(Mn)/m(Fe)	Process	w(Fe)/%	w(Mn)/%	w(Si)/%
0.5	Calculated from equilibrium phase diagram at 600 °C	0.72	0.20	8.26
	Measured from casting quenched at 600 °C after isothermal maintaining for 15 min	0.76	0.23	8.30
1.0	Calculated from equilibrium phase diagram at 600 °C	0.49	0.27	8.22
	Measured from casting quenched at 600 °C after isothermal maintaining for 15 min	0.51	0.32	8.27

From the results in Figs. 3 and 4, it was clear that the amount of the settled Fe-rich intermetallics was inversely proportional to the Fe content in the liquid. In other words, in order to obtain lower content in the liquid, more Fe should be settled at the bottom of the casting, which was essentially controlled by the initial Fe content and m(Mn)/m(Fe) ratio with holding temperature in solid−liquid co-existing region. As a result, the Fe-rich intermetallics solidified in the liquid phase and settled to the bottom of the cylinder casting would generate two types of materials. This was practically important as the top part could be harvested as recycled alloy for common engineering application, and the bottom part could be taken as special materials for different purposes. Clearly, two types of materials would show different characteristics of microstructure.

3.3 Microstructure of Al−Si−Cu−Fe alloy before and after sedimentation

Alloy A with m(Mn)/m(Fe)=1.0 was used to observe the microstructures before and after sedimentation. Figure 5 shows the optical micrograph of alloy A obtained in a d50 mm cylindrical casting continuously solidified from 650 °C. The primary α(Al) dendrites and interdendritic eutectic phases were observed in association with the presence of Fe-rich compounds showing dendritic morphology with different sizes from 10 μm to over 80 μm in Fig. 5(a). Three eutectic constituents were primarily observed in the interdendritic region, in which *A* showed Fe-rich compounds, *B* marked Si and *C* marked Al_2Cu phase in Fig. 5(b). Moreover, coarse irregularly-shaped intermediate phase was presented in Fig. 5(c). It was noted that Al_2Cu intermetallics were always associated with Fe-rich intermetallics. The EDX analysis confirmed that the Fe-rich intermetallics showed a typical constituent of $Al_{15}(Fe,Mn)_3Si_2$, as shown in Table 3 marked as original alloy.

In order to examine the microstructure of the casting after sedimentation, two samples were taken from the casting solidified at 600 °C after holding for 15 min for alloy A. One was taken at 4 mm from the top and the other was taken at 2 mm from the bottom of the casting on the longitudinal surface. The results were shown in Fig. 6. The microstructure of the retained alloy in Fig. 6(a) showed a much less Fe-rich phase in the matrix in comparison with that in the original alloy shown in Fig. 5(a). The presence of dendritic primary α(Al) phase was predominant in the matrix and only a few intermetallics were observed in the interdendritic area associated with eutectic constituent, which was similar to the phenomenon observed in the original alloy. However, coarse lamella-shaped precipitates of the intermediate phases in Fig. 5 were not observed in the sample after sedimentation in Fig. 6(a). The EDX analysis confirmed that the Fe-rich intermetallics were the same compound with a typical constituent of

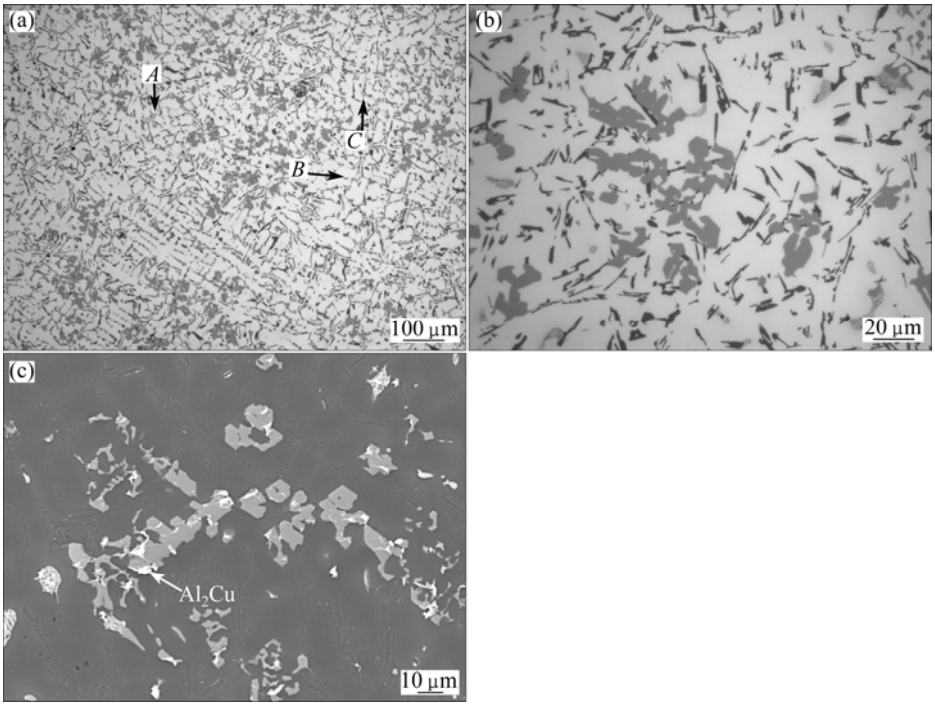

Fig. 5 Optical micrographs (a, b) and backscattered SEM micrograph (c) showing typical microstructure of *d*50 mm × 2500 mm casting made by alloy A

Table 3 Compositions of Fe-rich compounds identified by SEM-EDX for different samples

Sample	Identified compound	*x*/%				
		Al	Fe	Mn	Si	Cu
Original alloy	$Al_{13}(Fe,Mn)_3Si_2$	72.02	7.58	9.51	10.89	−
Retained alloy	$Al_{13}(Fe,Mn)_3Si_2$ $Cu_{0.6}$	70.41	10.29	5.52	10.75	3.13
Settled material	$Al_{13}(Fe,Mn)_3Si_2$	72.43	8.46	8.50	10.61	−

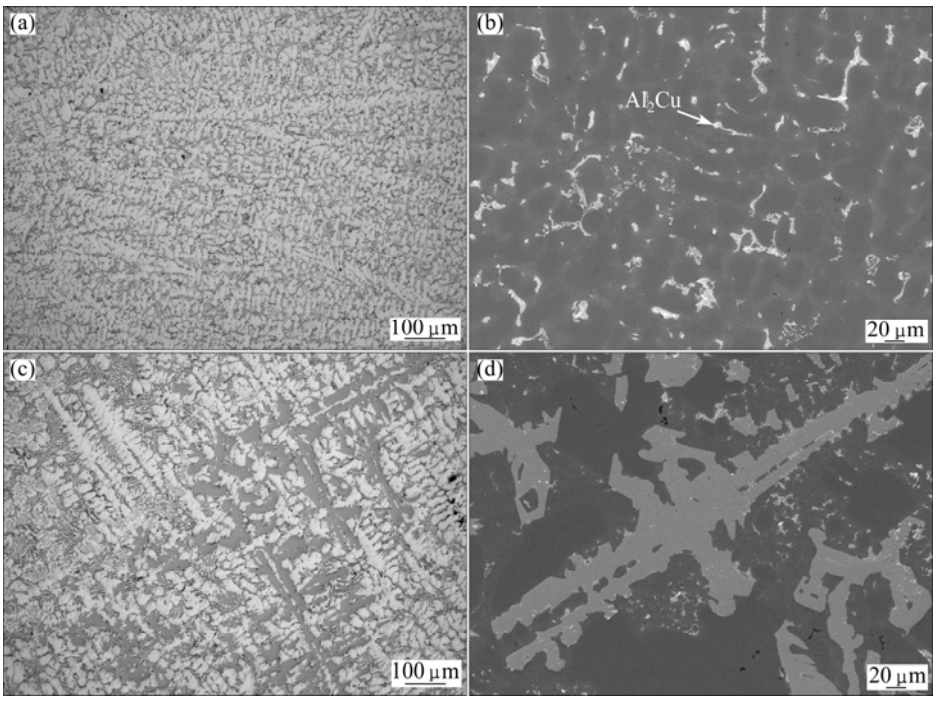

Fig. 6 Microstructures of retained alloy (a, b) and settled materials (c, d) obtained from *d*50 mm×2500 mm casting solidified after isothermal maintaining at 600 °C for 15 min

$Al_{15}(Fe,Mn)_3Si_2$ as shown in Table 3 marked as the retained alloy. The EDX spectrum also showed the presence of Al_2Cu phase in the interdendritic area, which was marked by the arrow in Fig. 6(b). On the other hand, the sedimentation material showed the significant enrichment of Fe-rich intermetallic phase, as shown in Fig. 6(c). The Fe-rich intermetallics in the sedimentation sample showed coarse dendritic morphology with obvious faceted characteristics at a size about 0.5 mm. The largest ones were several millimetres. These kinds of intermetallics were frequently observed in the microstructure in all samples after sedimentation. The EDX analysis confirmed that the Fe-rich intermetallics had the same compound with a typical constituent of $Al_{15}(Fe,Mn)_3Si_2$ as shown in Table 3 marked as the sedimentation material. In order to find out the element distribution in the Fe-rich intermetallics, a detailed SEM-EDX mapping was carried out for the Fe-rich intermetallics at the bottom of the cylindrical casting and the results were shown in Fig. 7. The mapped Fe-rich intermetallics phase was presented in Fig. 7(a), showing that the coarse dendrite was about 600 μm. The mapping images in Figs. 7(b)−(e) showed the contents of Al, Si, Mn and Fe in the intermetallics, respectively. Significant enrichment of Fe and Mn in the intermetallics was seen, but the enrichment of Si was not obvious. This was consistent with the results from the thermodynamics analysis and the composition analysis. It should be emphasized that the quantitative EDX results confirmed the existence of the same compound close to the stoichiometry of $Al_{15}(Fe,Mn)_3Si_2$ phase in the alloy before and after sedimentation. This confirmed that the constituent of the Fe-rich compounds was not changed in the sedimentation process.

4 Discussion

4.1 Solidification process and sedimentation of Fe-rich intermetallics

According to the thermodynamics calculation and the experimental results, two essential conditions to generate sedimentation of Fe-rich intermetallics are that the prior phase is Fe-rich intermetallics and the holding temperature is below the liquidus but above the solidus.

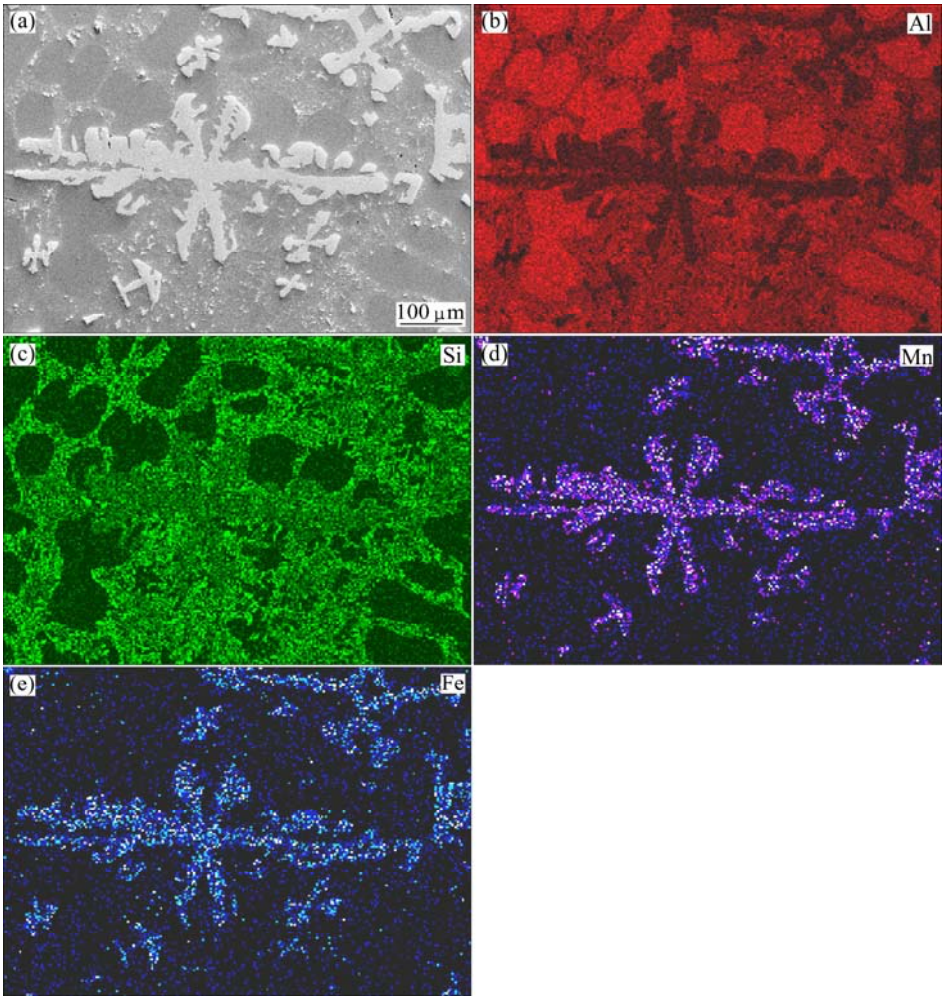

Fig. 7 SEM-EDX mapping for Fe-rich intermetallics obtained at bottom of *d*50 mm × 2500 mm cylindrical casting made by alloy A after isothermal maintaining at 600 °C for 15 min: (a) SEM image; (b) Al mapping; (c) Si mapping; (d) Mn mapping; (e) Fe mapping

If the holding temperature is higher than the liquidus, there is no solid Fe-rich intermediate phase to be formed. Similarly, if the prior phase is not Fe-rich intermetallics, the solid phase may be the mixture of different phases at the temperature below the liquidus but above the solidus. As it is known, the solubility of iron in liquid aluminium is 1.7% at eutectic temperature of 655 °C (even higher solubility at increased temperature), but it reduces to 0.05% in solid aluminium [5]. Therefore, most of the Fe-rich intermetallics are capable of precipitating during solidification. The addition of Mn into the melt plays an important role in guaranteeing the formation of α-AlFeMnSi as prior phase during solidification and minimising the balanced content of Fe in the retained melt. Therefore, the amount of Mn addition can be adjusted according to the requirement of Fe content in the retained melt and the initial content of Fe in the alloy. In the experimental Al−Si−Cu−Zn−Mn−Fe system, the addition of Mn can lower the balanced content of Fe after the precipitation of $Al_{15}(Fe,Mn)_3Si_2$ intermediate phase. During solidification, the growth of $Al_{15}(Fe,Mn)_3Si_2$ is controlled by diffusion, which is a function of the holding time. It is generally believed that the increased size of the intermetallics will also promote the sedimentation because of the increased mass. Meanwhile, it should be noted that the reduction of the holding temperature can also increase the amount of intermetallics precipitation, which not only reduces the balanced content of Fe in the melt, but also increases the sedimentation efficiency. Consequently, lower iron content can be achieved in the retained alloys.

In the experimental alloy, lots of $Al_{15}(Fe,Mn)_3Si_2$ intermetallics as primary phases have consumed other elements in the pre-defined stoichiometric proportion. Therefore, one expected that the reduction of Fe content is associated with that of Mn simultaneously. Therefore, the addition of elements in the initial alloy should be properly controlled by considering the composition of alloy to satisfy the specification requirement. It is ideal that the additions of different elements can be consumed during the precipitation of $Al_{15}(Fe,Mn)_3Si_2$ phase. After the processing for Fe removal, the alloy composition is still within the specification requirement. It is also important to note that the sedimentation of Fe-rich intermetallics is not associated to Cu and Zn. Therefore, Cu and Zn contents are not changed during sedimentation of Fe-rich intermetallics.

4.2 Sedimentation process

The sedimentation of solid particles in a liquid is caused by the variation of density. This can be calculated with physical fundamentals. The buoyant force (F_b) on the particle can be defined as

$$F_b = V'\rho g = \frac{m\rho g}{\rho'} \tag{1}$$

where m is the mass of particle, ρ is the density of liquid, V' is the volume of particle, ρ' is the density of solid particle, and g is the gravitational acceleration as a constant. The gravitational or external force F_g is defined as

$$F_g = mg \tag{2}$$

The drag force F_D or frictional resistance on the moving body can be defined as

$$F_D = C_D \frac{v^2}{2} \rho A \tag{3}$$

where v is the velocity of falling, C_D is the drag coefficient, and A is the area.

The resultant force on the falling body is

$$m\frac{dv}{dt} = F_g - F_b - F_D \tag{4}$$

Therefore,

$$m\frac{dv}{dt} = mg - \frac{m\rho g}{\rho'} - C_D \frac{v^2}{2} \rho A \tag{5}$$

The falling of the body consists of two periods: the period of accelerated fall and constant-velocity fall. The acceleration period is usually very short. Hence, the period of constant-velocity fall is the important one, in which $dv/dt=0$. Therefore, the falling speed v_t can be described as

$$v_t = \sqrt{\frac{2mg(\rho' - \rho)}{A\rho' C_D \rho}} \tag{6}$$

Assuming the particles are in spherical shape, $m=\pi D'^3\rho'/6$, $A=\pi D'^2/4$, where D' is the size of particles, therefore,

$$v_t = \sqrt{\frac{4gD'(\rho' - \rho)}{3C_D \rho}} \tag{7}$$

The drag coefficient for rigid spheres has been shown to be a function of the Reynolds number. In the laminar-flow region, the drag coefficient is defined as [16]

$$C_D = \frac{24}{D'\rho v / \mu} \tag{8}$$

Therefore,

$$v_t = \frac{gD'^2(\rho' - \rho)}{18\mu} \tag{9}$$

Equation (9) can be used to calculate the falling speed of Fe-rich particles. The data for the calculation of falling speed are presented in Table 4 [17−19]. The

calculated results indicate that the falling speed is 0.031 mm/s for a 10 μm spherical particle and is 1.99 mm/s for a 80 μm spherical particle, indicating a 64 times difference when these particles fall a same height. For the experimental condition, a 10 μm particle formed at the top of the melt in a 250 mm long tube can be theoretically settled to the bottom in 8065 s, but the settle time is only 125.57 s for a 80 μm particle formed at the same location. However, the experiments showed that the sedimentation time of Fe-rich particles was between 600 and 900 s. This may be because the shape of the solid Fe-rich intermetallics is not in spherical and the entrapped liquid in the dendrite arms will affect the sedimentation process. On the other hand, the solid Fe-rich intermetallics have a wide range of sizes, which spread from few micrometres to several millimetres. And the location to form solid Fe-rich intermetallics is also varied to the maximum falling distance of 250 mm. Therefore, the sedimentation time will be different. In addition, it is also obvious that the sedimentation is actually determined by the size, density of solid particles, and the density and viscosity of melt. The larger particles with higher density will promote higher falling rate.

Table 4 Relevant parameters used for calculation of sediment rate of $Al_{15}(Fe,Mn)_3Si_2$ intermetallics in aluminium melt

Parameter	Value	Ref.
Density of liquid aluminium at 660 °C, ρ/(g·cm^{-3})	2.4	[17]
Viscosity of pure aluminium at 660 °C, μ/(10^{-3} N·s·m^{-2})	1.4	[18]
Density of solid AlFeMnSi, ρ'/(g·cm^{-3})	3.2	[19]

5 Conclusions

1) The introduction of Mn into an aluminium alloy containing high contents of Fe and Si is an effective approach to lower the Fe level in the equilibrium liquid phase after sedimentation at a temperature interval between its liquidus and solidus. The higher Mn/Fe mass ratio results in the lower Fe content in the retained alloy, during which manganese is also consumed and settled at the bottom of the melt as solid Fe-rich intermetallics. Therefore, the final Fe content can be controlled by the variation of manganese content and holding temperature of the melt.

2) The sedimentation of Fe-rich intermetallics in the Al−Si−Cu−Fe alloy can be achieved within a relatively short period of time. The most of Fe-rich intermetallics can be settled at 600 °C after 10 min. The reduction of Fe content in the retained alloy is 31.4% when m(Mn)/m(Fe)=0.5 and 53.3% when m(Mn)/m(Fe)=1.0 in the original alloy.

3) The settled Fe-rich intermediate phase should be controlled as α-AlFeMnSi phase, typically $Al_{15}(Fe,Mn)_3Si_2$ in the Al−Si−Cu−Fe alloy, which provides the lower balanced Fe content in the melt in comparison with other Fe-rich intermetallics.

Acknowledgements

The financial support from TSB (UK) under project No. 101172 is acknowledged. The authors also would like to thank the EPSRC (UK) and Jaguar Cars Ltd. (UK) for financial support under the grant for the EPSRC Centre - LiME.

References

[1] WANG L, MAKHLOUF M, APELIAN D. Aluminium die casting alloys: Alloy composition, microstructure, and properties-performance relationships [J]. International Materials Reviews, 1995, 40: 221−238.

[2] JI S, WATSON D, FAN Z, WHITE M. Development of a super ductile diecast Al−Mg−Si alloy [J]. Materials Science and Engineering A, 2012, 556: 824−833.

[3] KHALIFA W, SAMUEL F H, GRUZLESKI J E. Iron intermetallic phases in the Al corner of the Al−Si−Fe system [J]. Metallurgical and Materials Transactions A, 2003, 34: 807−825.

[4] ALLEN C M, O′REILLY K A Q, CANTOR B, EVANS P V. Intermetallic phase selection in 1xxx Al alloys [J]. Progress in Materials Science, 1998, 43: 89−170.

[5] DAVIS J R. ASM speciality handbook: Aluminium and aluminium alloys [M]. Ohio: ASM International, 1993.

[6] JI S, YANG W, GAO F, WATSON D, FAN Z. Effect of iron on the microstructure and mechanical property of Al−Mg−Si−Mn and Al−Mg−Si diecast alloys [J]. Materials Science and Engineering A, 2013, 564: 130−139.

[7] ZHANG L, GAO J, DAMOAH L N W, ROBERTSON D G. Removal of iron from aluminum: A review [J]. Mineral Processing and Extractive Metallurgy Review: An International Journal, 2012, 33: 99−157.

[8] SKJERPE P. Intermetallic phases formed during DC-casting of an Al−0.25 Wt Pct Fe−0.13 Wt Pct Si alloy [J]. Metallurgical and Materials Transactions A, 1987, 18: 189−200.

[9] MONDOLFO L F. Aluminium alloys: Structure and properties [M]. London: Butterworth, 1976.

[10] CACERES C H, DAVIDSON C J, GRIFFITHS J R, WANG Q G. The effect of Mg on the microstructure and mechanical behavior of Al−Si−Mg casting alloys [J]. Metallurgical and Materials Transactions A, 1999, 30: 2611−2617.

[11] MUNSON D. A clarification of the phases occurring in aluminium-rich aluminium-iron-silicon alloys with particular reference to the ternary phase alpha-AlFeSi [J]. Journal of the Institute of Metals, 1976, 95: 217−219.

[12] COUTURE A. Iron in aluminium casting alloys—A literature survey [J]. International Cast Metals Journal, 1981, 6: 9−17.

[13] JORSTAD J L. Understanding “sludge” [J]. Die Casting Engineer, 1986, 11−12: 30−36.

[14] GOBRECHT J. Gravity segregation of iron, manganese, and chromium in Al−Si foundry alloys [J]. Foundry, 1977, 367: 171−173. (in French)

[15] CHEN S L, DANIEL S, ZHANG F, CHANG Y A, YAN X Y, XIE F Y, SCHMID-FETZEF R, OATESD W A. The PANDAT software package and its applications [J]. Calphad, 2002, 26: 175−188.

[16] PATWARDHAN V S, TIEN C. Sediment and liquid fluidization of solid particles of different sizes and densities [J]. Chemical Engineering Science, 1985, 40: 1051−1060

[17] BRANDES E A, BROOK G B. Smithells metals reference book [M]. 7th ed. Oxford: Butterworth, 1992.

[18] BATTEZZATI L, GREER A L. The viscosity of liquid metals and alloys [J]. Acta Metallurgica, 1989, 37: 1791−1802.

[19] FLORES A, TOSCANO J A, RODRIGUEZ S, SALINAS A, NAVA E. Microstructure formation of Al−Fe−Mn−Si aluminides by pressure-assisted reactive sintering of elemental powder mixtures [J]. Advanced Materials Research, 2009, 68: 21−23.